Permeability of Subcritical Hydrocarbons in Activated Carbon

Jun-Seok Bae and D. D. Do
Division of Chemical Engineering, The University of Queensland, St. Lucia, QLD 4072, Australia

DOI 10.1002/aic.10313
Published online in Wiley InterScience (www.interscience.wiley.com).

A new diffusion and flow model is presented to describe the behavior of hydrocarbon vapors in activated carbon. The micro/mesopore size distribution (PSD) is obtained according to Do's method which consists of two sequential processes of pore layering and pore filling. This model uses the micro/meso PSD obtained from each adsorbate equilibrium isotherm, which reflects the dynamics behavior of adsorbing molecules through the solid. The initial rise in total permeability is mainly attributed to adsorbed-phase diffusion (that is, surface diffusion), whereas the decrease over reduced pressure of about 0.9 is attributed to the reduction of pore space available for gas phase diffusion and flow. A functional form of surface diffusivity is proposed and validated with experimental data. This model predicts well the permeability of condensable hydrocarbon vapors in activated carbon. © 2005 American Institute of Chemical Engineers *AIChE J,* 51: 487–501, 2005

Introduction

Activated carbon is a carbonaceous adsorbent with a highly developed internal pore structure that depends on raw materials and activation techniques. Generally activated carbon has a wide range of pore size distribution (PSD): a graphitic structure (micropore) and the interspace (mesopore and macropore) between graphitic units (Do, 1998). Because the transport of adsorbing molecules in activated carbon takes place in a wide range of pore sizes from micropore to macropore, the PSD is required to determine the dynamic behavior of adsorbing molecules through the pores. The PSD is a statistical and representative term of individual pores, extracted from the adsorption behavior of adsorbate in a porous medium. Assuming that the local isotherm function $\Psi(P, H)$ and measured adsorbed concentration $C_\mu(P)$ (mol/g) are available, we can determine the PSD from the following relation:

$$C_\mu(P) = \int_{\sigma_{ss}}^{\infty} \Psi(P, H)\, f(H) dH \tag{1}$$

Correspondence concerning this article should be addressed to D. D. Do at duongd@cheque.uq.edu.au.

where $f(H)$ ($m^3/g \cdot m$) is the distribution function of pore size with H being physical pore width, which is the distance between opposite centers of the two outermost carbon layers. With the PSD function $f(H)$, the total flux J_T ($mol/m^2 \cdot s$) through the solid is given by

$$J_T = \frac{\rho_p}{\tau} \int_{\sigma_{ss}}^{\infty} J_P(P, H)\, f(H) dH \tag{2}$$

where $J_P(P, H)$ is the flux in each pore of the solid and ρ_p (Kg/m^3) is the particle density of the solid (kg/m^3). The tortuosity τ accounts for the deviation between real pore geometry and ideal pore shape. Thus the PSD is closely associated with the equilibrium and kinetic properties of the solid (Lopez-Ramon et al., 1997).

It is noted, however, that the local isotherm function $\Psi(P, H)$ must be assumed to derive the PSD, which thus depends on $\Psi(P, H)$. For porous media such as activated carbon, a number of assumptions in terms of pore shape, surface roughness, interference of functional groups, pore connectivity, and intermolecular potential model are involved in $\Psi(P, H)$ (Do and Do, 2003). In this regard, the "effective" PSD is an appropriate term to use. Furthermore, as Seaton and coworkers have stressed (Liu et al., 1994; Lopez-Ramon et al., 1997; Murray et

al., 1999), the choice of adsorbate with a given $\Psi(P, H)$ of the solid affects the PSD because of the different accessibilities of adsorbate molecules to each pore. This indicates a significant point that the PSD, obtained from equilibrium isotherms of an adsorbate, reflects the corresponding mass transfer of the adsorbate through the solid. Therefore, the PSD is a "respective" term as well.

Once the respective pore size distribution of each adsorbate is obtained, the transport processes of condensable vapors through the pores are considered. The steady-state total flux J_T in Eq. 2 for a given pressure gradient imposed across two ends of the medium is simply described by

$$J_T = -B_T(P, H)\frac{\partial P}{\partial z} \qquad (\text{mol/m}^{-2}\cdot\text{s}) \tag{3}$$

where $B_T(P, H)$ is the total permeability across the medium, which can be easily obtained from permeation experiments. It has been well established that the total permeability through activated carbon at a given pressure gradient is attributed to four transport processes such as Knudsen diffusion (B_K), gaseous viscous flow (B_V), adsorbed-phase diffusion (B_μ), and capillary condensate flow (B_C)

$$B_T = B_K + B_V + B_\mu + B_C \qquad (\text{mol/m}\cdot\text{s}\cdot\text{Pa}) \tag{4}$$

Unlike the others, the adsorbed-phase diffusion remains less understood. Although a number of transport models for condensable vapors through a porous medium have been suggested (Do et al., 2001; Kainourgiakis et al., 1996; Lee and Hwang, 1986; Tzevelekos et al., 1998), none of them can reasonably describe what we have observed (that is, the lower B_K than expected, and the initial sharp increase in B_T) (Bae and Do, 2002, 2003a,b). Based on our observations, we propose and validate a diffusion and flow model of condensable vapors in activated carbon in this article, taking into account the effect of the PSD.

Theory

The micro/meso PSD is determined according to Do's method and each transport mechanism through the pores is established in the following subsections. It is noted that, because the macro PSD is based on cylindrical pore shape and the micro/meso PSD is assumed all pores to be slit pores, the transport processes in micro/mesopores and in macropores are determined with the respective pore shape assumptions.

Respective micro/meso PSD

Here we are dealing with transport of molecules through activated carbon. Thus the relative PSD of each adsorbate is more important than the absolute PSD of the solid. Herein we take the local isotherm function $\Psi(P, H)$ from Do and coworkers (Do and Do, 2002; Do et al., 2001) because of its simplicity in application. Here we briefly summarize their method. We take a slit-pore model such that pores are composed of two parallel lattice planes with sublattice layers underneath each lattice layer; this is a more realistic micropore configuration for activated carbon. In pores with confined geometry, the pore pressure can be significantly enhanced as a result of the overlapping of the potential energies exerted by two lattice planes. Also the adsorption affinity is greater and subsequently the statistical thickness is thicker in the pores.

Potential energy $\varphi(z)$

The potential energy of interaction between a molecule and carbon surface, which is usually taken to follow the Steele 10-4-3 potential, can be described in terms of z being the distance between a molecule center and the center of the outermost carbon layer

$$\varphi(z) = 4\pi\rho_s\sigma_{sf}^2\varepsilon_{sf}\Delta\left\{\frac{1}{5}\left(\frac{\sigma_{sf}}{z}\right)^{10} - \frac{1}{2}\left(\frac{\sigma_{sf}}{z}\right)^{4}\left[1 + \frac{z}{3\Delta(1 + 0.61\Delta/z)^3}\right]\right\} \tag{5}$$

where ρ_s is the density of carbon center and Δ is the distance between sublattice layers in each lattice plane; σ_{sf} (collision diameter) and ε_{sf} (well depth) are fluid–solid molecular parameters, which can usually be estimated from the Lorentz–Berthelot rule. Thus the potential energy exerted by two opposite walls is given by

$$\varphi_p(z) = \varphi(z) + \varphi(H - z) \tag{6}$$

Pore pressure P_P

In a confined geometry, such as micropore arising from the overlapping of the potential energies exerted by opposite pore walls, the pore pressure is enhanced and greater than the corresponding bulk pressure. Taking the potential energy E_0 at the pore center as a representative energy for compressing molecules within the pore (Do et al., 2001), we have the pore pressure P_P as follows

$$P_P = P\exp\left(-\frac{\alpha E_0(H)}{R_g T}\right) \tag{7}$$

where the factor α accounts for the overestimation of the pore pressure in very small pores. The exponential term in the right-hand side of Eq. 7 is called an enhancement factor E_n.

Local isotherm function $\Psi(P, H)$

For the molecular layering process, we account for the fluid–solid interaction by taking a Brunauer–Emmett–Teller (BET)–type equation. By allowing the potential enhancement in the BET constant and in the pore pressure, the statistical thickness of adsorbed layer is given by

$$\frac{t}{t_m} = \frac{C_{\text{BET\_}P}x_P}{(1 - x_P)[1 + (C_{\text{BET\_}P} - 1)x_P]} \tag{8a}$$

where x_P is the reduced pore pressure and t_m is the monolayer thickness that can be calculated from $t_m = (v_M/N_A)^{1/3}$, where v_M is the liquid molar volume of the adsorbed phase (m^3/mol) and N_A is the Avogadro number. The BET constant C_{BET_P} of a pore is related to the BET constant C_{BET_S} of a flat surface as follows

$$\frac{C_{BET\_P}}{C_{BET\_S}} = \exp\left(\frac{Q_P(H) - Q_S}{R_g T}\right) \tag{8b}$$

where Q_S and $Q_P(H)$ are the heats of adsorption for a flat surface and a pore having a width H, respectively. The heat of adsorption is considered as the well depth of potential energy, which can be obtained from Eqs. 5 and 6 for each case, respectively (Do et al., 2001).

This pore layering process is followed by the pore filling process at the reduced critical pore pressure x_C (that is, P_{PC}/P_0), which is governed by the Kelvin equation for a slit pore, as follows

$$\frac{H}{2} - t - z_0 = \frac{\gamma v_M}{R_g T \ln(1/x_C)} \tag{9}$$

where γ is the surface tension (N/m) and z_0 is the half collision diameter of a carbon atom (that is, $z_0 = \sigma_{ss}/2$). Provided that the adsorbed phase behaves like a liquid phase (that is, the molar density of the adsorbed phase is constant in either multilayered pores or in filled pores), the local isotherm function is thus given by

$$\Psi(P, H) = \begin{cases} \dfrac{1}{v_M}\dfrac{t}{(H/2 - z_0)} & \text{for } x_P < x_C \\ \dfrac{1}{v_M} & \text{for } x_P > x_C \end{cases} \tag{10}$$

Having known the observed adsorbed concentration C_μ (mol/g) and the local isotherm function $\Psi(P, H)$ (mol/m^3), we are ready to derive the respective PSD by inverting Eq. 1. Because activated carbon is known not to conform to any analytical continuous distribution functions, a discrete pore size distribution is obtained by minimizing the following residuals

$$R = \sum_{j=1}^{m}\left(\sum_{i=0}^{n}\Psi(P_j, H_i)W_i - C_{\mu j}\right)^2 \quad \text{with}$$
$$j = 1, 2, \ldots, m \text{ and } i = 1, 2, \ldots, n \tag{11}$$

where W_i is the volume of pore i (m^3/g) and $C_{\mu j}$ is the adsorbed concentration (mol/g) at a given pressure point j.

Transport processes

The real pore shape of activated carbon does not conform strictly to either a slit or a cylinder. In terms of pore shape for molecular transport, we assume that micro/mesopores have a slit shape, as assumed to determine the micro/meso PSD, whereas macropores are cylindrical in shape to determine the macro PSD from mercury porosimetry. Because activated carbon has a wide range of pore sizes, one would not expect that the four transport processes mentioned earlier always take place at any given pressure in each pore. That is, adsorbed-phase diffusion is a dominant process in micropores where most adsorption takes place, whereas Knudsen diffusion and viscous flow control the transport of molecules in macropores where surface diffusion is negligible and condensate flow does not occur (except when the reduced pressure approaches unity). On the other hand, the four processes take place in mesopores, depending on loading. This is illustrated schematically in Figure 1.

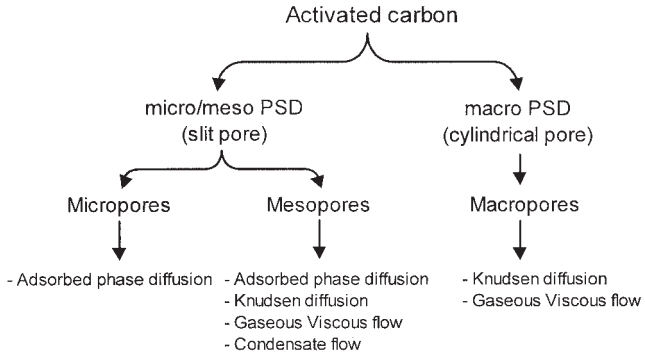

Figure 1. Diffusion and flow in a wide range of pore sizes of activated carbon.

As well as the dependency of the transport processes on pore sizes, the bulk pressure also determines the occurrence of the processes at a given temperature. Denoting r the distance from the pore center to the surface of the solid atoms [that is, $r = (H - \sigma_{ss})/2$, where σ_{ss} is the collision diameter of the solid atom] and P_C the critical pressure (at which pores are filled with adsorbate), we consider three transport modes:

(1) $P_P < P_C$ and $t < t_m < r$: The pore pressure is less than the critical pressure and the statistical thickness is less than the monolayer thickness t_m. In this case three transport processes take place: adsorbed-phase diffusion, Knudsen diffusion, and gaseous viscous flow.

(2) $P_P < P_C$ and $t_m < t < r$: When t is greater than t_m but less than r, the same processes to the above case still take place. However it is assumed in this case that the adsorbed-phase diffusion is contributed only by the uppermost adsorbed molecules (Okazaki et al., 1981). This assumption is logical because it is hard for the adsorbed molecules underneath the uppermost ones to move unless the neighboring ones move. That is, the driving force for surface diffusion is the concentration gradient of the uppermost adsorbed molecules.

(3) $P_P > P_C$ and $t < r < r_C$: When P_P is greater than P_C, pores are filled with adsorbed molecules. In this case only capillary condensate flow takes place.

These transport modes are depicted schematically in Figure 2. In the following subsections, each of the transport processes is considered in detail.

Knudsen Diffusion. For diffusion and flow of subcritical hydrocarbons in activated carbon, it has been stressed that Knudsen diffusivity (and subsequently Knudsen diffusion permeability) is a function of loading (Bae and Do, 2003a). By introducing a collision reflection factor f, defined as the fraction of molecules undergoing collision to the solid surface over

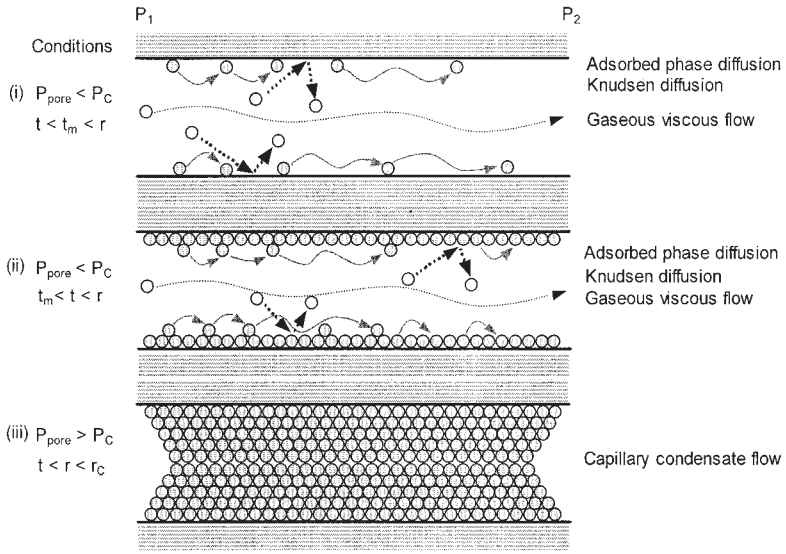

Figure 2. Diffusion and flow of adsorbing molecules according to pore pressure and statistical thickness in a pore of activated carbon.

reflection from the solid surface, we have the pore Knudsen diffusivity of subcritical hydrocarbons as follows

$$D_K = \frac{4K_0(r)}{3}\sqrt{\frac{8R_gT}{\pi M}}\left(\frac{2-f_P}{f_P}\right) \tag{12}$$

where $K_0(r)$ is the Knudsen diffusion parameter, which is a function of pore shape as follows (Nicholson and Petropoulos, 1985)

$$K_0(r) = \begin{cases} 3r/8 & \text{for slit pores with } r \text{ being pore half width} \\ r/2 & \text{for cylindrical pores with } r \text{ being pore radius} \end{cases} \tag{13}$$

The collision reflection factor f_P in a pore is given as a function of monolayer fractional loading θ_{Pm} in the pore

$$f_P(P, r) = f_\infty\theta_{Pm} + f_0(1 - \theta_{Pm}) \qquad (f_\infty < f_0) \tag{14}$$

where f_∞ and f_0 are the collision reflection factors at high pressure (close to the vapor pressure, P_0) and at the limit of zero pressure, respectively. The monolayer fractional loading θ_{Pm} in pores can be calculated from the statistical thickness (in Eq. 8a)

$$\theta_{Pm} = \begin{cases} t/t_m & \text{for } t < t_m \\ 1 & \text{for } t \geq t_m \end{cases} \tag{15}$$

Denoting $f(r)$ (m^3/ g · m) the pore size distribution in terms of accessible pore half width r (m) (that is, $r = H/2 - \sigma_{ss}/2$), we have the Knudsen diffusion permeability contributed by all pores available at a given pressure gradient as follows:

$$B_K(P) = \left(\frac{\rho_P}{\tau_K}\right)\left(\frac{16}{3\sqrt{2\pi MR_gT}}\right)\int_{r_C(P)}^{\infty} K_0(r-t) \times \left(\frac{2-f_P}{f_P}\right)R_0(r, t)f(r)dr \qquad (r > t) \tag{16}$$

where $(r - t)$ is the empty pore half width and τ_K is the tortuosity corresponding to Knudsen diffusion. $R_0(r, t)$ corresponds to the pore volume reduction arising from layering of adsorbing molecules on the pores, which has the following forms for slit pores and cylindrical pores, respectively

$$\left(\frac{r-t}{r}\right) \qquad \text{and} \qquad \left(\frac{r-t}{r}\right)^2$$

Because we has a discrete pore size distribution of $f(r)$, the total B_K can be calculated by replacing the integral of Eq. 16 with a summation of B_K over all pore ranges. At a given pressure, Eq. 16 is rewritten as

$$B_K(P) = \left(\frac{\rho_P}{\tau_K}\right)\left(\frac{16}{3\sqrt{2\pi MR_gT}}\right)\sum_{i=r_C}^{\infty} K_0(r_i - t_i) \times \left(\frac{2-f_{Pi}}{f_{Pi}}\right)R_0(r_i, t_i)W_i \qquad (r > t) \tag{17}$$

where W_i (m^3/g) is the pore volume of pore size i, which is equal to $f(r_i)\Delta r_i$.

Gaseous Viscous Flow. Gaseous viscous flow is relatively well known. Because of the presence of adsorbed molecules on the solid surface the cross-sectional area available for transport is reduced at moderate or high pressures. The gaseous viscous

flow over an entire range of pore sizes at a given pressure gradient is given by

$$B_V(P) = \left(\frac{\rho_P}{\tau_V}\right)\left(\frac{P}{\mu_g R_g T}\right)\int_{r_C}^{\infty} B_0(r-t)\,R_0(r,\,t)\,f(r)dr \qquad (r > t) \quad (18)$$

where μ_g is the gas phase viscosity of adsorbate and τ_V is the tortuosity corresponding to gaseous viscous flow. $B_0(r)$ is the viscous flow parameter, which is a function of pore shape as follows (Nicholson and Petropoulos, 1985)

$$B_0(r) = \begin{cases} r^2/3 & \text{for slit pores} \\ r^2/8 & \text{for cylindrical pores} \end{cases} \qquad (19)$$

Similarly at a given pressure with a range of discrete pore sizes, Eq. 18 can be expressed in a discrete form as

$$B_V(P) = \left(\frac{\rho_P}{\tau_V}\right)\left(\frac{P}{\mu_g R_g T}\right)\sum_{i=rc}^{\infty} B_0(r_i - t_i)\,R_0(r_i,\,t_i)\,W_i \qquad (r > t) \quad (20)$$

Adsorbed-phase Diffusion. Having known the total permeability B_T and the gas phase permeability (that is, B_K and B_V), the difference between them is contributed by adsorbed-phase diffusion as well as capillary condensate flow. Thus denoting the difference as the apparent adsorbed-phase diffusion permeability B_{app}, we have

$$B_{app} = B_T - (B_K + B_V) = B_\mu + B_C \qquad (21)$$

where B_μ and B_C are the permeabilities corresponding to adsorbed-phase diffusion (that is, surface diffusion) and condensate flow, respectively. The surface diffusion flux can be expressed as a Fickian-type equation in terms of a gas-phase pressure gradient along the direction of pore length

$$J_\mu = -\frac{\rho_p}{\tau_\mu} D_\mu^* \frac{C_\mu}{P}\frac{\partial P}{\partial z} \qquad (\text{mol/m}^2 \cdot \text{s}) \qquad (22)$$

where D_μ^* is the corrected surface diffusivity, which is a function of loading; τ_μ is the tortuosity corresponding to surface diffusion; and C_μ is the adsorbed concentration (mol/g). Taking C_μ from Eq. 1 and the local isotherm function Ψ from Eq. 10, we have the surface diffusion permeability B_μ as

$$B_\mu(P) = \left(\frac{\rho_P}{\tau_\mu \nu_M}\right)\int_{r_C}^{\infty} D_\mu^*(P,\,r)\,\frac{\psi^E(P,\,r)}{P} f(r)dr \qquad (23)$$

where $\psi^E(P, r)$ is the effective local isotherm function for surface diffusion. Because the uppermost adsorbed molecules are actually responsible for the surface diffusion as proposed earlier, $\psi^E(P, r)$ can be given by

$$\psi^E(P,\,r) = \begin{cases} t/r & \text{for } t \le t_m \\ t_m/r & \text{for } t > t_m \end{cases} \qquad (t < r) \qquad (24)$$

Thus at a given bulk pressure, Eq. 23 is given by

$$B_\mu(P) = \left(\frac{\rho_P}{\tau_\mu \nu_M}\right)\sum_{i=r_C}^{\infty} D_\mu^*(P,\,r_i)\,\frac{\psi^E(P,\,r_i)}{P}\,W_i \qquad (25)$$

The functional form of the corrected surface diffusivity D_μ^* will be proposed in detail under Results and Discussion.

Capillary Condenstate Flow. When the pore pressure P_P is greater than the critical pressure P_C, capillary condensation or pore filling takes place. Assuming that the condenstate behaves like a Newtonian fluid, such that the viscosity remains unchanged across the pore, and that there is no slip flow on the solid surface [that is, $v_z(r) = 0$], we can describe the capillary condenstate flow at a given pressure as follows

$$B_C(P) = \left(\frac{\rho_P}{\tau_C}\right)\left(\frac{R_g T}{3\mu_L \nu_M^2}\right)\sum_{i=1}^{r_C}\frac{r_i^2}{P}\,W_i \qquad (26)$$

where μ_L is the liquid viscosity of adsorbate, which is assumed to be independent of gas-phase pressure and τ_C is the tortuosity corresponding to the capillary condensate flow.

So far we have established all necessary equations to describe the transport processes of adsorbing vapors in activated carbon.

Experimental

Subcritical hydrocarbons including benzene, carbon tetrachloride, and *n*-hexane were used to investigate diffusion and flow mechanisms in a commercial activated carbon, which has the following physical properties: particle density 733 kg/m^3, total porosity 0.71, and BET surface area 1.2×10^6 m^2/kg. The physical properties of the adsorbates and their Lennard–Jones potential parameters are listed in Table 1 and in Table 2, respectively.

The setup of permeation experiment and the procedures can be found elsewhere (Bae and Do, 2002). An activated carbon cell was mounted, separating two reservoirs, one of which is much larger than the other so that the pressure P_1 in the larger reservoir is practically kept constant during the course of diffusion and adsorption. The pressure P_2 in the smaller reservoir was monitored with respect to time up to the equilibrium pressure P^*. The total permeability B_T of adsorbate through the cell was calculated by plotting the following equation

$$\ln\left(\frac{P_1 - P^*}{P_1 - P_2(t)}\right) = B_T\left(\frac{AR_g T}{V_2 L}\right)t \qquad (27)$$

where V_2 is the smaller reservoir volume, A is the cross-sectional area of the sample, and L is the sample length.

Table 1. Physical Properties of Adsorbates Studied

Adsorbate	Temp. (K)	MW (kg/kmol)	LMV* (m^3/kmol)	Liquid Viscosity (Pa · s)	Vapor Viscosity (Pa · s)	Surface Tension (N/m)	Vapor Pressure (Pa)
C_6H_6	293	78.11	8.928×10^{-2}	6.108×10^{-4}	7.442×10^{-6}	0.02887	9983
	303		9.030×10^{-2}	5.638×10^{-4}	7.694×10^{-6}	0.02755	15,852
	312		9.126×10^{-2}	5.050×10^{-4}	7.921×10^{-6}	0.02637	23,318
CCl_4	293	153.82	9.691×10^{-2}	9.739×10^{-4}	9.820×10^{-6}	0.02691	12,138
	303		9.803×10^{-2}	8.450×10^{-4}	1.015×10^{-6}	0.02567	18,898
	312		9.909×10^{-2}	7.491×10^{-4}	1.045×10^{-6}	0.02459	27,354
n-C_6H_{14}	293	86.18	1.291×10^{-1}	3.100×10^{-4}	6.355×10^{-6}	0.01854	16,232
	303		1.309×10^{-1}	2.846×10^{-4}	6.585×10^{-6}	0.01743	25,076
	312		1.327×10^{-1}	2.651×10^{-4}	6.791×10^{-6}	0.01645	36,024

*LMV, liquid molar volume.

Results and Discussion

Respective micro/meso pore size distribution

The optimization of Eq. 11 is effectively conducted with built-in functions in MatLab software to determine the respective micro/mesopore volumes of the solid. The respective pore volume reflects the accessibility of adsorbing molecules to the pores, which in turn affects the transport of molecules through the pores. Knowing the pore volumes for each adsorbate, the respective PSD can be obtained in terms of pore width, shown in Figures 3, 4, and 5 for benzene, carbon tetrachloride, and *n*-hexane, respectively, at 303 K. The respective PSD for benzene is slightly different from that for carbon tetrachloride in the micropore range, whereas *n*-hexane shows a distinctly different PSD in the mesopore range from that for the others. Based on each PSD at 303 K, the equilibrium isotherms of each adsorbate at two other temperatures are predicted and plotted in Figures 3, 4, and 5 with respective PSDs. Generally the predictions are fairly good. Small deviations at low pressures could be attributable either to experimental errors or to the slightly different accessibility of adsorbing molecules to the pores at different temperatures, giving rise to a small deviation in the micropore range of the respective PSD at different temperatures (not shown).

It has been well established in the literature that the PSDs obtained by using equilibrium isotherms of different molecules are different with a given solid, depending on the type of the molecules used (Lopez-Ramon et al., 1997). Beside uncertainties in pore shape, fluid–fluid and fluid–solid interaction parameters, and surface heterogeneity, adsorbing molecules having different molecular size and structure may have different degrees of accessibility to the pore space. For instance, using the PSD obtained from benzene adsorption isotherm at 312 K, we predict the isotherm for *n*-hexane at the same temperature as shown in Figure 6. Likewise we use the PSD obtained from *n*-hexane and predict the benzene isotherm, and the results are also shown in the same figure. It is clearly seen that the adsorption isotherms based on the benzene PSD are overestimated at low pressures, whereas the *n*-hexane PSD gives rise to underestimation of adsorption isotherms. This point suggests that smaller molecules have higher accessibility to the pore space than larger ones at low pressures, which may reflect the transport of adsorbing molecules through the pores. Therefore the PSD should be obtained respectively for adsorbing molecules to better describe their dynamics behavior through the pores.

Macropore size distribution

The macropore size distribution of the activated carbon was obtained by a mercury intrusion porosimetry technique (Gray, 1991). The pore diameter D_p was determined according to the Washburn equation, assuming pore shape to be cylindrical

$$D_P = -4\gamma_m \cos\theta / P \tag{28}$$

where γ_m is the surface tension of mercury (0.485 N/m) and θ is the contact angle (140°). The pore diameter is replaced by the physical pore width H (that is, $H = D_p + \sigma_{ss}$).

The macropore size distribution is plotted against the physical pore width in Figure 7 in the form of a histogram. The macro PSD will be used to calculate Knudsen diffusion per-

Table 2. Lennard–Jones Potential Parameters, and BET and Henry Constants for Flat Surface

Adsorbate	Temp. (K)	Collision Diameter* (m)	ε/k* (K)	C_{BET_S}**	Henry Constant** (mol/m^2 · Pa)
C_6H_6	293	5.349×10^{-10}	412.3	44.18	2.43×10^{-8}
	303			41.17	1.12×10^{-8}
	312			38.62	8.89×10^{-9}
CCl_4	293	5.947×10^{-10}	322.7	26.22	8.72×10^{-8}
	303			24.00	8.73×10^{-9}
	312			22.18	4.12×10^{-9}
n-C_6H_{14}	293	5.949×10^{-10}	399.3	217.59	5.71×10^{-8}
	303			185.97	3.10×10^{-8}
	312			162.12	1.87×10^{-8}

* Poling et al., 2001.
**Do and Do, 2002.

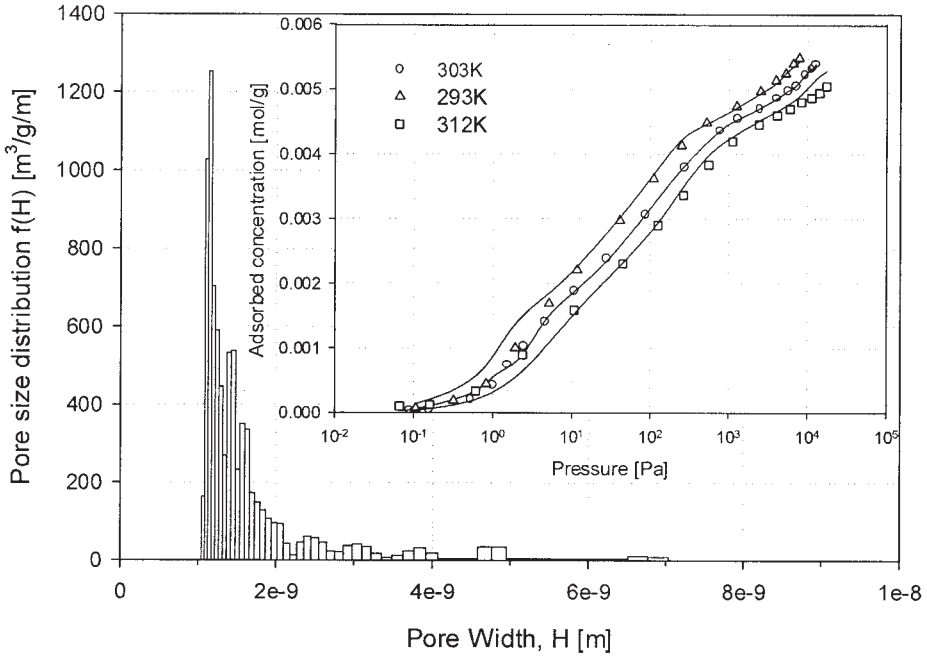

Figure 3. Respective micro/mesopore size distribution of an Ajax activated carbon, obtained from the equilibrium isotherm of benzene at 303 K.

The equilibrium isotherms of benzene at 293 and 312 K are predicted with the above pore size distribution.

meability B_K and gaseous viscous flow permeability B_V in macropores according to Eqs. 17 and 20, respectively.

Permeability of condensable vapors

The total permeability (B_T) of condensable vapors through activated carbon is calculated according to Eq. 27 and depicted in terms of reduced pressure in Figure 8. The behavior of B_T against reduced pressure (RP) shows three distinct characteristics as follows:

(1) $0 < \mathrm{RP} < 0.1$: B_T increases sharply at very low pressures. This sharp increase should correspond to the transport of molecules in micropores because gas-phase diffusion is insig-

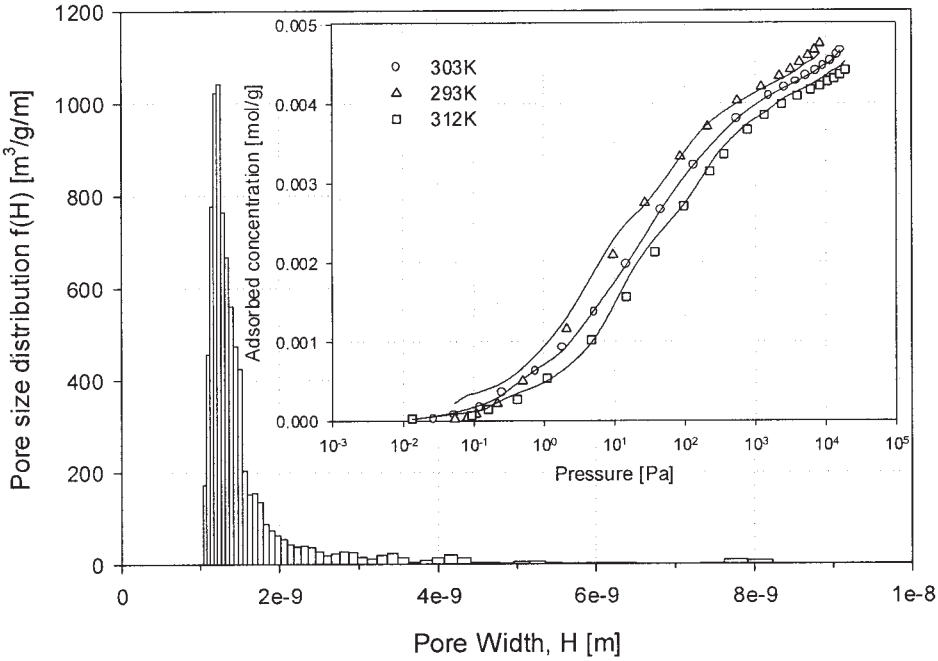

Figure 4. Respective micro/mesopore size distribution of an Ajax activated carbon, obtained from the equilibrium isotherm of CCl_4 at 303 K.

The equilibrium isotherms of CCl_4 at 293 and 312 K are predicted with the above pore size distribution.

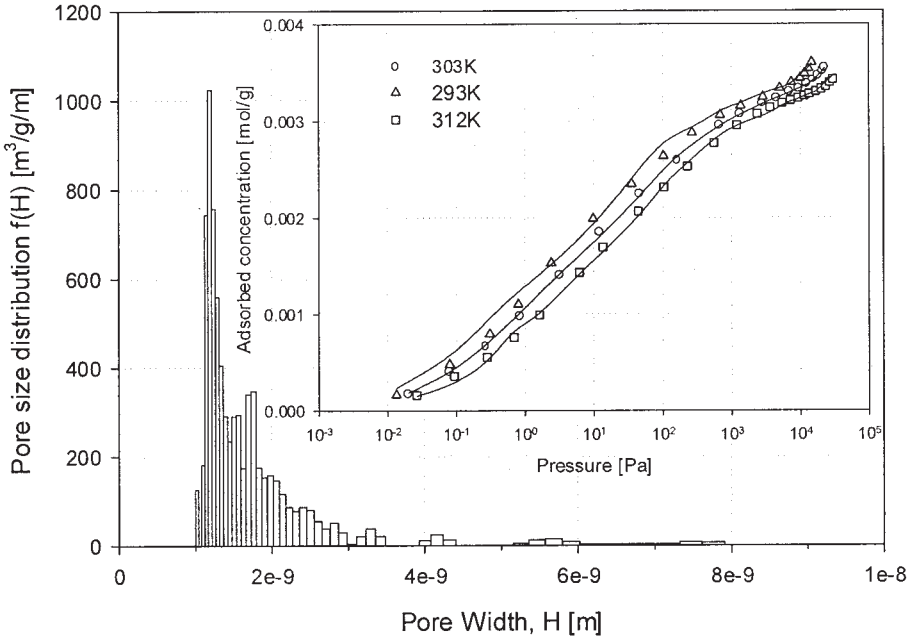

Figure 5. Respective micro/mesopore size distribution of an Ajax activated carbon, obtained from the equilibrium isotherm of *n*-hexane at 303 K.

The equilibrium isotherms of *n*-hexane at 293 and 312 K are predicted with the above pore size distribution.

nificant compared with the adsorbed-phase diffusion in micropores where the adsorbed concentration increases sharply at very low pressures. Once micropores are completely filled, the contribution of adsorbed-phase diffusion decreases as a result of the reduction of the concentration gradient inside pores.

(2) $0.1 < RP < 0.8$: As pressure increases gas-phase diffusion dominates the transport of molecules through macropores, leaving the contribution of adsorbed-phase diffusion in small pores insignificant. Thus the total permeability is almost a linear function of pressure within this range of pressure.

(3) $RP > 0.9$: Although macropores are not completely filled, the total permeability starts to decrease around reduced pressure of 0.9, regardless of the type of adsorbate attributed to the reduction of pore volume.

Gas-phase diffusion and flow

Knudsen diffusion permeability (B_K) and gaseous viscous flow permeability (B_V) are calculated according to Eqs. 17 and 20, respectively. They are dependent on pore size, pore volume, and bulk pressure as shown against pore half width (or radii for cylindrical pores) in Figures 9 and 10. The product of

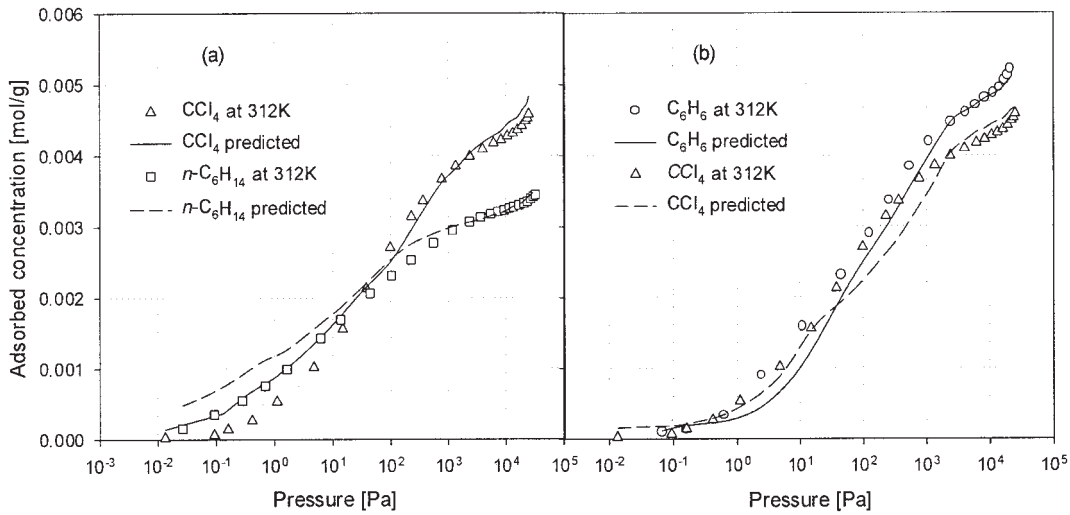

Figure 6. Prediction of equilibrium isotherms.

(a) Carbon tetrachloride and *n*-hexane at 312 K obtained from the PSD based on benzene at 312 K, and (b) benzene and carbon tetrachloride at 312 K obtained from the PSD based on *n*-hexane at 312 K.

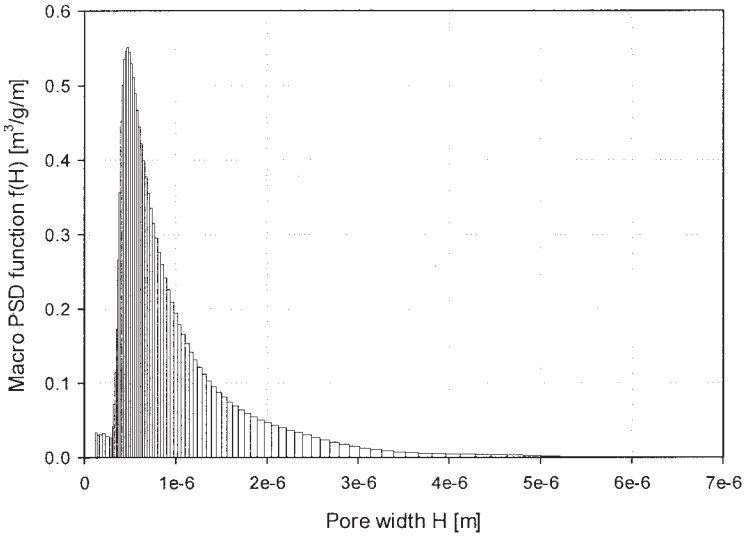

Figure 7. Macropore size distribution of an Ajax activated carbon, obtained by a mercury intrusion porosimetry technique.

pore volume and empty pore half width [that is, $(r - t)$ for B_K and $(r - t)^2$ for B_V] at a given pressure gives the unique shapes of B_K and B_V at each pore size. The first hump at pore half width of about 5×10^{-7} m arises from the maximum macropore volume in Figure 7. The second and the third humps in Figure 10 are attributed to the product of macropore volume and empty pore half width. As pore size approaches its maximum, the contribution of B_K and B_V to the total permeability decreases as a result of the small pore volume. It is clearly seen that most gas-phase diffusion and flow take place in macropores. The contribution of mesopores to them is noticeable only at low pressures. Although the pore layering process reduces the pore volume for gaseous flow and diffusion as bulk pressure increases, most macropore space is still available for gas-phase diffusion and flow, resulting in an increase in B_V with bulk pressure. Similarly B_K increases up to a certain pressure at which the monolayer fractional loading θ_{Pm} in pores is unity (that is, $t = t_m$) and then becomes independent of bulk pressure, giving rise to a slight decrease in B_K with bulk pressure because of the deduction of pore space.

From the respective micro/mesopore size distributions, the fraction of pore numbers available for gas-phase diffusion and flow can be obtained for slit pores with an assumption of pore length, width, and breadth being uncorrelated (Seaton, 1991)

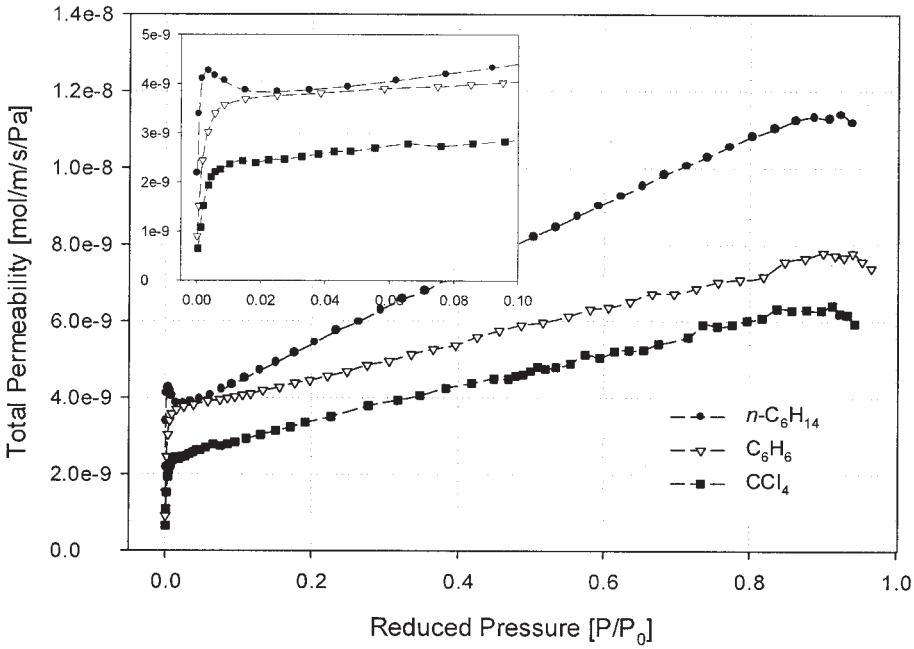

Figure 8. Total permeabilities of *n*-hexane, benzene, and carbon tetrachloride against reduced pressure in activated carbon at 303 K.

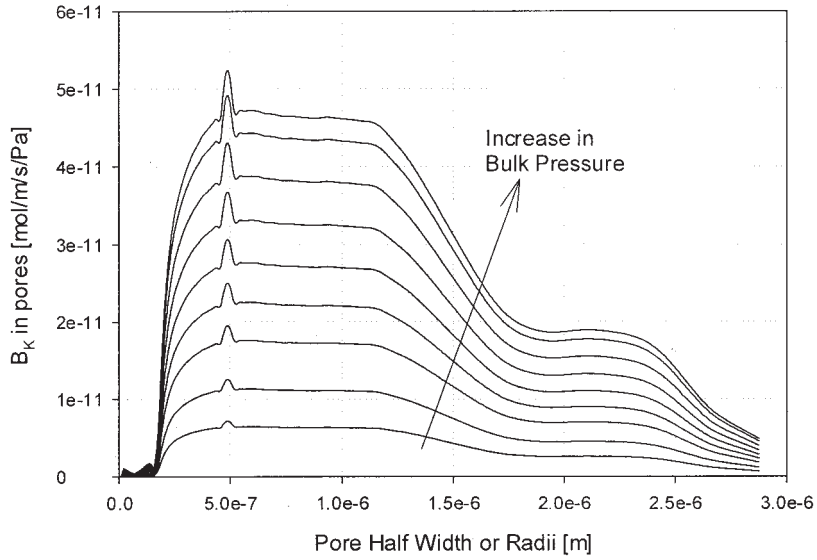

Figure 9. Knudsen diffusion permeability of benzene in the pores of activated carbon at bulk pressures of 3.4 (bottom), 90.7, 238.6, 396.3, 611.9, 927.1, 1351.2, 1851.2, and 3513.7 Pa (top).

$$g(P) = \frac{\int_{H^*}^{\infty} \frac{f(H)}{H}\, dH}{\int_{0}^{\infty} \frac{f(H)}{H}\, dH} \tag{29}$$

where H^* is the critical pore width below which pores are completely filled. Figure 11 shows the normalized pore number distributions $g(P)$ of condensable vapors against reduced pressure. At very low pressures (that is, less than reduced pressure of 0.02), $g(P)$ of *n*-hexane decreases faster than that of the others, which reflects the accessibility of *n*-hexane molecules to micro/mesopores. This could be a consequence of the difference in the molecular size and shape. At reduced pressure of around 0.9, no mesopores are available for gas-phase diffusion and flow as indicated in Figure 11.

Condensate flow

Before we propose the functional form of the corrected surface diffusivity D^*_μ, we first consider the condensate flow of which process is well established in Eq. 26. Because of geometric restriction on mass transfer through the pores, the condensate flow is restricted in small pores, depending on the pore size, by taking the following relation

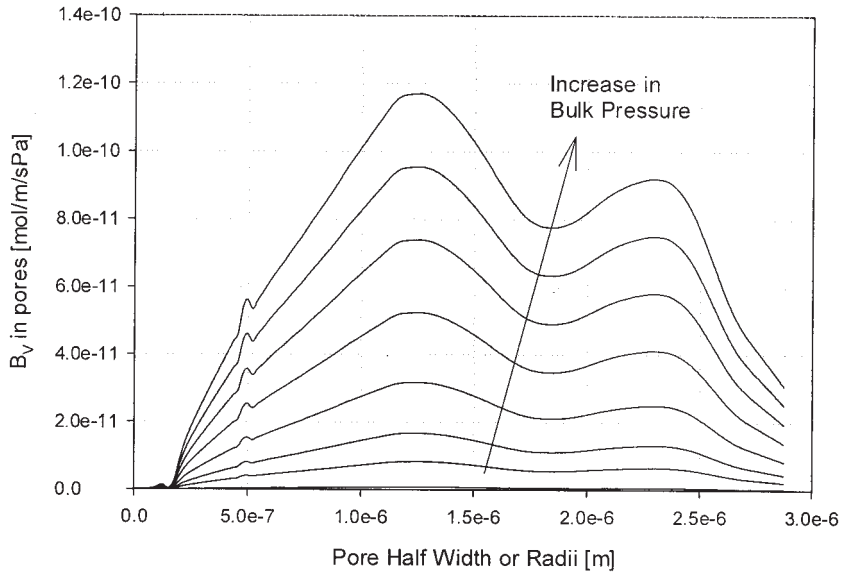

Figure 10. Gaseous viscous flow permeability of benzene in the pores of activated carbon at bulk pressures of 3.4 (bottom), 90.7, 924.1, 1851.2, 3513.7, 5795.5, 8179.3, 10,565.1, and 12,974.2 Pa (top).

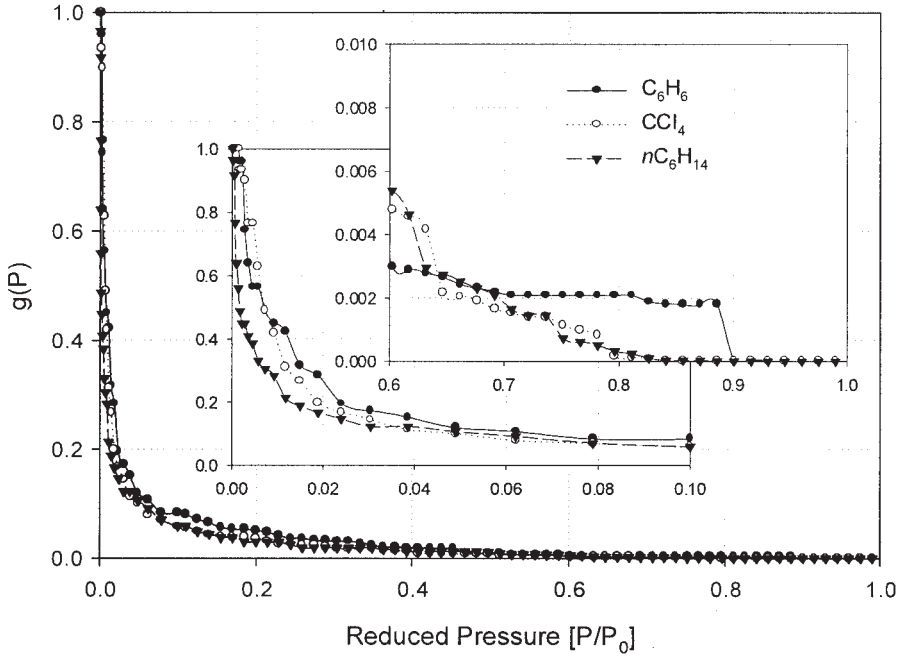

Figure 11. Plot of normalized pore number distributions of benzene, carbon tetrachloride, and *n*-hexane in the micro/mesopore range of activated carbon at 303 K.

$$B_C(P) = \left(\frac{\rho_P}{\tau_C}\right)\left(\frac{R_g T}{3\mu_L \nu_M^2}\right) \sum_{i=1}^{rc} \frac{r_i^2}{PE_n(r_i)} W_i \qquad (30)$$

where E_n is the enhancement factor defined in Eq. 7, which is significant only in small pores. Also if the pore size is smaller than the collision diameter of the adsorbing molecule, no condensate flow is allowed. Because it is reasonable to assume that the contribution of surface diffusion to the total permeability at high pressure is insignificant, the apparent adsorbed-phase diffusion permeability B_{app} is mainly contributed by the condensate flow at high pressure. Thus τ_C can be obtained by matching B_C with B_{app}. Figure 12 shows the condensate flow permeability in terms of adsorbed concentration in pores. When micropores are completely filled, the contribution of that kind (if it exists) to the total permeability should not be termed adsorbed-phase diffusion nor condensate flow because the driving force for the former is diminished and the latter mainly occurs in mesopores. Nevertheless, for computational purposes here we treated that kind of contribution as condensate flow with a geometric restriction (that is, the enhancement factor). The first peak of

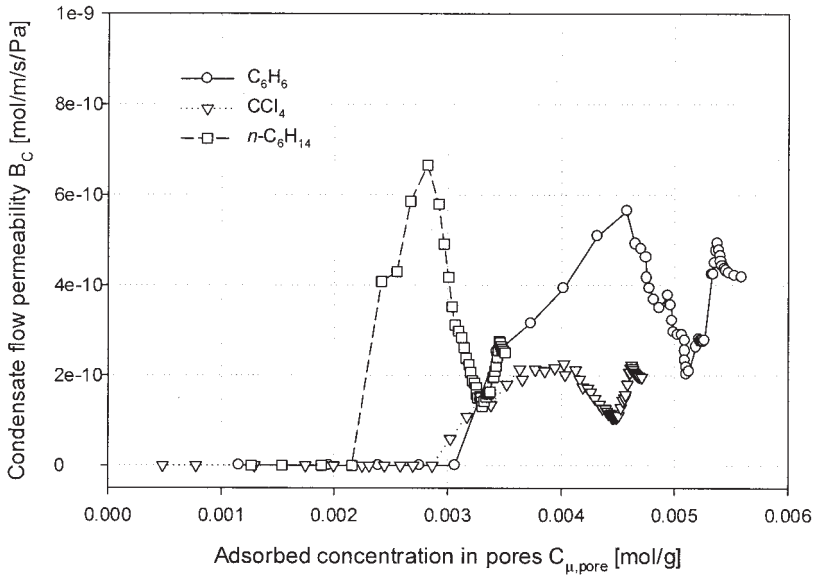

Figure 12. Plots of condensate flow permeability against adsorbed concentration in pores for benzene, carbon tetrachloride, and *n*-hexane in activated carbon at 303 K.

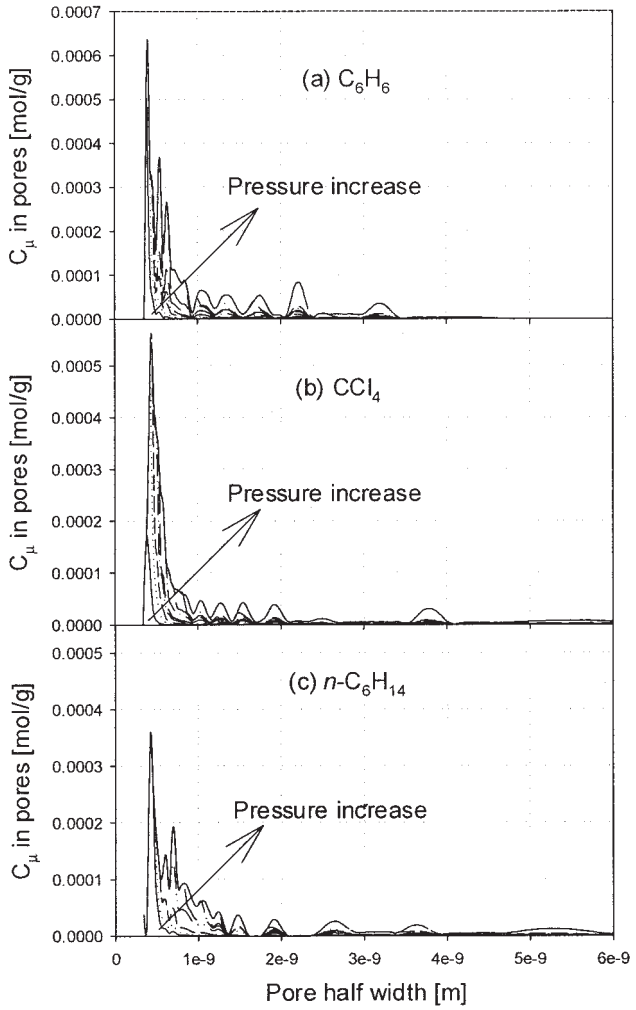

Figure 13. Plots of adsorbed concentration of benzene (a), carbon tetrachloride (b), and *n*-hexane (c) in micro/mesopores against pore half width.

B_C in Figure 12 corresponds to the contribution in micropores and the second to that in mesopores.

Adsorbed-phase diffusion

Adsorbed concentration in each pore ($C_{\mu,pore}$) is calculated and depicted against pore half width in Figure 13, according to the local isotherm function and the respective pore size distribution. As one would expect, the pore adsorbed concentration follows the shape of the respective pore size distribution (PSD) as pressure increases. The slightly different $C_{\mu,pore}$ peaks in position reflect the different degrees of accessibility of adsorbate to pore space, which makes the interpretation of the PSD and $C_{\mu,pore}$ more complicated without taking into account pore connectivity. Seaton and coworkers over the last decade have made significant efforts to determine the pore connectivity of a porous medium from the PSD and adsorption/desorption isotherms of different kinds (Lopez-Ramon et al., 1997; Murray et al., 1999; Seaton, 1991). However, according to the IUPAC hysteresis loop classification, the type of an Ajax activated carbon falls into an H4 hysteresis loop, which exhibits a scanty difference between adsorption and desorption isotherms, giving rise to a very high value of connectivity for the Ajax activated carbon, which is nonphysical. In spite of the importance of pore connectivity in molecular transport, because of the complexity in constructing the real pore shape and size, and in defining consequent transport processes in activated carbon, little has been known on the quantified role of the connectivity in each transport process mentioned. Because the tortuosity in pore capillary models can be understood as the connectivity in a pore network structure (Kainourgiakis et al., 1996), herein we take a parallel capillary model to describe transport phenomena in activated carbon.

Now we are in the position to extract the functional form of D^*_μ from the surface diffusion permeability B_μ (which is equal to $B_T - B_K - B_V - B_C$). Because of the geometric restriction on molecular transport in very small pores, pores smaller than the fluid–solid collision diameter (σ_{sf}) are assumed to make no contribution to the mass transfer of adsorbed molecules through activated carbon particle. From the behavior of B_μ in terms of fractional loading in pores and pore pressure, we propose the following functional form of D^*_μ

$$D^*_\mu = D^*_{\mu 0}\frac{1}{1-\theta_P}(1+\beta P_P) \tag{31}$$

where $D^*_{\mu 0}$ is the surface diffusivity at zero loading and θ_P is the fractional loading in pores. Thus the surface diffusion permeability can be given by

$$B_\mu(P) = \left(\frac{\rho_P D^*_{\mu 0}}{\tau_\mu \nu_M}\right)\int_{r_C}^{\infty}\left(\frac{1}{1-\theta_P}\right)(1+\beta P_P)\frac{\psi^E}{P}f(r)dr \tag{32}$$

Assuming that adsorbed-phase diffusion and condensate flow take place through the same pathway, the tortuosity τ_μ is treated as τ_C. The fitting parameters $D^*_{\mu 0}$ and β are obtained by comparing experimental data with model results and listed in Table 3. As the corrected surface diffusivity at zero loading in Table 3 suggests, molecular size plays an important role in surface diffusion. On the other hand, the response of surface diffusivity to pressure, which is reflected in β, shows an opposite trend to molecular size.

The permeabilities of benzene, carbon tetrachloride, and *n*-hexane in terms of adsorbed concentration in pores are plotted in Figures 14, 15, and 16, respectively. It can be seen clearly that the initial rise in the total permeability is mainly the result of surface diffusion. The prediction of hydrocarbon permeability in activated carbon according to our model fits fairly well the experimental data. Surface diffusion dominates molecular transport at low pressures, whereas gaseous diffusion and flow mostly contribute to the total permeability at moderate and high pressures. It is interesting to see than the surface diffusion permeability of *n*-hexane after its maximum drops faster that of the others, giving rise to a minimum appearance

Table 3. Parameters for Surface Diffusivity in Eq. 31 for Adsorbates Studied at 303 K

Parameter	C_6H_6	CCl_4	n-C_6H_{14}
$D^*_{\mu 0}$ (m^2/s)	1.039×10^{-11}	4.249×10^{-12}	3.222×10^{-12}
β (1/Pa)	2.005	4.352	6.326

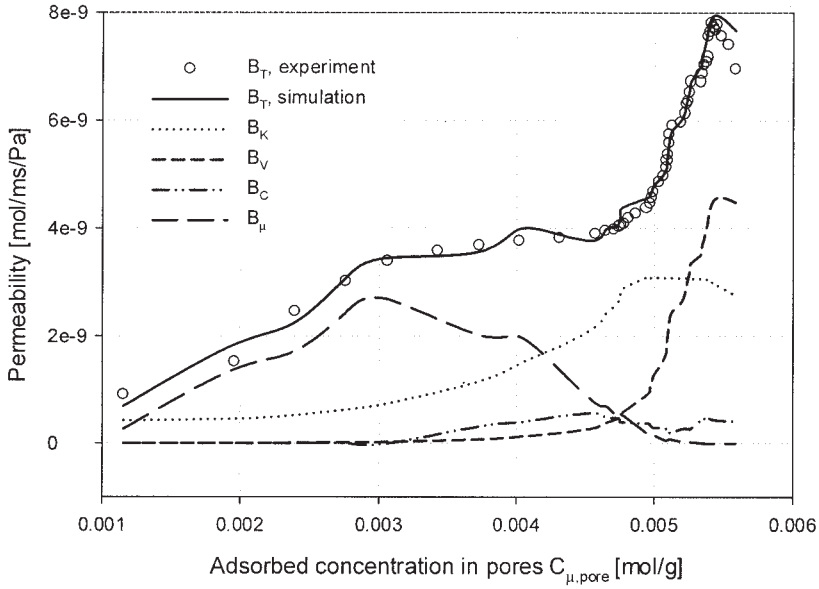

Figure 14. Permeabilities of benzene with respect to adsorbed concentration in the pores of activated carbon at 303 K.

in the total permeability. The inconsistent existence of a minimum in the specific flow rate vs. pressure curve has been reported in the literature (Ash and Grove, 1960). Considerable literature has suggested tentative or numerical explanations on the minimum behavior, concluding that the minimum appears in the transition region where both Knudsen diffusion and gaseous viscous flow are expected to control the transport. In the case of activated carbon, which has a large portion of micropores as well as macropores, however, it is shown herein that the minimum appearance in total permeability is mainly attributed to the behavior of surface diffusion with respect to adsorbed concentration in pores.

Conclusions

By incorporating the respective micro/mesopore size distribution of each adsorbate and the macropore size distribution we have established and validated a new diffusion and flow model to describe the permeation behavior of condensable hydrocarbon vapors in a commercial activated carbon, which has large portion of micropores as well as macropores. The initial rise in total permeability mainly results from surface diffusion and gaseous diffusion and flow dominate transport at moderate and high pressures. The decrease in total permeability over reduced pressure of about 0.9 is found to be attributed

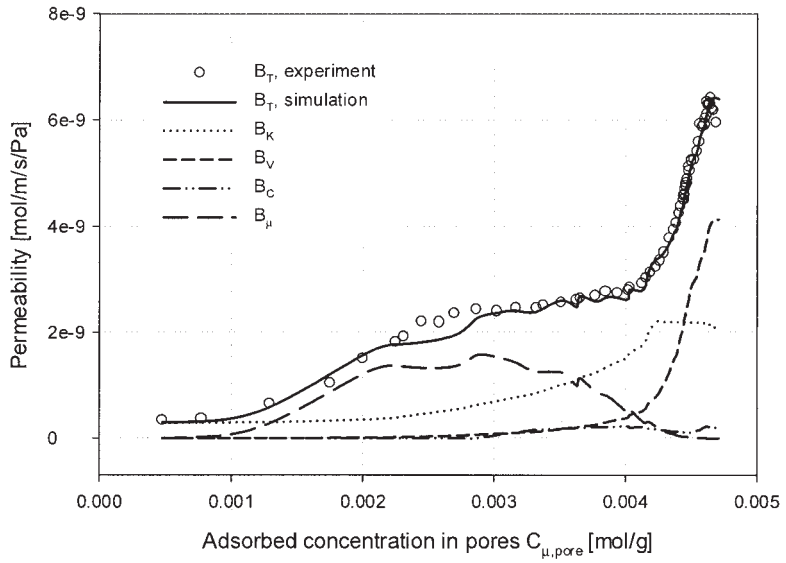

Figure 15. Permeabilities of carbon tetrachloride with respect to adsorbed concentration in the pores of activated carbon at 303 K.

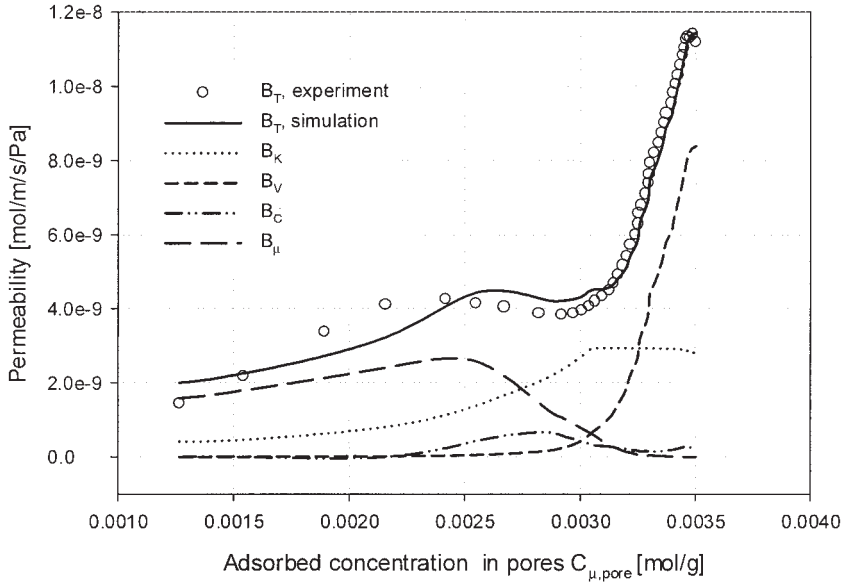

Figure 16. Permeabilities of *n*-hexane with respect to adsorbed concentration in the pores of activated carbon at 303 K.

to the reduction of pore space for gas phase diffusion and flow, as indicated clearly in Figure 14. Furthermore, the corrected surface diffusivity proposed herein accounts for interaction between adsorbing molecules and the solid surface, and the solid pore size (which is reflected to pore pressure). The present model has demonstrated that the prediction of permeability is in substantial agreement with experimental data.

Acknowledgments

The support from the Australian Research Council is gratefully acknowledged.

Notation

B = viscous flow parameter, m^2
B_k, B_v = permeabilities for Knudsen diffusion and viscous flow, respectively, mol/m · s · Pa
B_T, B_μ = total permeability and surface diffusion permeability, respectively, mol/m · s · Pa
C_{BET} = BET constant
C_μ = adsorbed concentration, mol/g
D_μ, D^*_μ = surface diffusivity and corrected surface diffusivity, respectively, m^2/s
f_P = collision reflection factor in pores
H = pore width, m
J = molar flux, mol/m^2 · s
K = Knudsen diffusion parameter, m
P, P = gas phase pressure and vapor pressure, respectively, Pa
Q = heat of adsorption, J/mol
R_g = gas constant, J/mol · K
t = statistical thickness, m
T = temperature, K
W = pore volume, m^3/g

Greek letters

Δ = distance between sublattice layers in each lattice plane, m
Ψ = local isotherm function, mol/m^3
γ = surface tension, N/m
φ = potential energy, J/mol
μ_g, μ_L = viscosity in gas phase and in liquid phase, respectively, Pa·s
ν_m = liquid molar volume, m^3/mol
θ_{Pm} = monolayer fractional loading in pores
ρ_s, ρ_p = surface carbon center density, no. of center/m^3 and carbon particle density, kg/m^3
σ = collision diameter, m
τ_k,τ_v,τ_s,τ_c = tortuosity corresponding to Knudsen diffusion, gaseous viscous flow, surface diffusion, and condensate flow, respectively

Literature Cited

Ash, R., and D. M. Grove, "Low-Pressure Gas Flow in Consolidated Porous Media," *Trans. Faraday Soc.*, **56**, 1357 (1960).
Bae, J.-S., and D. D. Do, "Study on Diffusion and Flow of Benzene, *n*-Hexane and CCl_4 in Activated Carbon by a Differential Permeation Method," *Chem. Eng. Sci.*, **57**, 3013 (2002).
Bae, J.-S., and D. D. Do, "Surface Diffusion of Strongly Adsorbing Vapors in Activated Carbon by a Differential Permeation Method," *Chem. Eng. Sci.*, **58**, 4403 (2003a).
Bae, J.-S., and D. D. Do, "A Unique Behavior of Sub-Critical Hydrocarbon Permeability in Activated Carbon at Low Pressures," *Korean J. Chem. Eng.*, **20**, 1097 (2003b).
Do, D. D., *Adsorption Analysis: Equilibria and Kinetics*, Imperial College Press, London (1998).
Do, D. D., and H. D. Do, "Effects of Adsorbate–Adsorbate Interaction in the Description of Adsorption Isotherm of Hydrocarbons in Micro-Mesoporous Carbonaceous Materials," *Appl. Surf. Sci.*, **196**, 13 (2002).
Do, D. D., and H. D. Do, "Refined Method of Potential Enhancement in the Equilibria Characterization of Activated Carbon: Comparison with GCMC and DFT," *Langmuir*, **19**, 8302 (2003).
Do, D. D., C. Nguyen, and H. D. Do, "Characterization of Micro-Meso porous Carbon Media," *Colloids Surf. A: Physicochem. Eng. Aspects*, **187–188**, 51 (2001).
Gray, P. G., "Fundamental Studies of Sorption Dynamics of SO_2, NO_2, and CO_2 on Activated Carbon," PhD Thesis, The University of Queensland, Brisbane, Australia (1991).
Kainourgiakis, M. E., A. K. Stubos, N. D. Konstantinou, N. K. Kanellopoulos, and V. Milisic, "A Network Model for the Permeability of Condensable Vapors through Mesoporous Media," *J. Membr. Sci.*, **114**, 215 (1996).
Lee, K.-H., and S.-T. Hwang, "The Transport of Condensable Vapors through a Microporous Vycor Glass Membrane," *J. Colloid Interface Sci.*, **110**, 544 (1986).
Liu, H. L., L. Zhang, and N. A. Seaton, "Characterization of Mesoporous Solids Using Sorption Hysteresis Measurements," *Characterization of Porous Solids III*, J. Rouquerol, F. Rodriguez-Reinos, K. S. W. Sing, and K. K. Unger, eds., *Stud. Surf. Sci. Catal.*, **87**, 129 (1994).
Lopez-Ramon, M. V., J. Jagiello, T. J. Bandosz, and N. A. Seaton,

"Determination of the Pore Size Distribution and Network Connectivity in Microporous Solids by Adsorption Measurements and Monte Carlo Simulation," *Langmuir*, **13**, 4435 (1997).
Murray, K. L., N. A. Seaton, and M. A. Day, "Use of Mercury Intrusion Data, Combined with Nitrogen Adsorption Measurements, as a Probe of Pore Network Connectivity," *Langmuir*, **15**, 8155 (1999).
Nicholson, D., and J. H. Petropoulos, "Calculation of the Surface Flow of a Dilute Gas in Model Pore from First Principles. Part III. Molecular Gas Flow in Single Pores and Simple Model Porous Media," *J. Colloid Interface Sci.*, **106**, 538 (1985).
Okazaki, M., H. Tamon, and R. Toei, "Interpretation of Surface Flow Phenomenon of Adsorbed Gases by Hopping Model," *AIChE J.*, **27**, 262 (1981).
Poling, B. E., J. M. Prausnitz, and J. P. O'Connell, *The Properties of Gases and Liquids*, McGraw-Hill, New York (2001).
Seaton, N. A., "Determination of the Connectivity of Porous Solids from Nitrogen Sorption Measurements," *Chem. Eng. Sci.*, **46**, 1895 (1991).
Tzevelekos, K. P., E. S. Kikkinides, A. K. Stubos, M. E. Kainourgiakis, and N. K. Kanellopoulos, "On the Possibility of Characterizing Mesoporous Materials by Permeability Measurements of Condensable Vapors: Theory and Experiments," *Adv. Colloid Interface Sci.*, **76–77**, 373 (1998).

Manuscript received Feb. 4, 2004, and revision received May 28, 2004.